Environ. Sci. Technol. **2006**, *40,* 3865−3871

Water Structure and Aqueous Uranyl(VI) Adsorption Equilibria onto External Surfaces of Beidellite, Montmorillonite, and Pyrophyllite: Results from Molecular Simulations

JEFFERY A. GREATHOUSE* AND RANDALL T. CYGAN

Geochemistry Department, Sandia National Laboratories, Albuquerque, New Mexico 87185-0754

Molecular dynamics simulations were performed to provide a systematic study of aqueous uranyl adsorption onto the external surface of 2:1 dioctahedral clays. Our understanding of this key process is critical in predicting the fate of radioactive contaminants in natural groundwaters. These simulations provide atomistic detail to help explain experimental trends in uranyl adsorption onto natural media containing smectite clays. Aqueous uranyl concentrations ranged from 0.027 to 0.162 M. Sodium ions and carbonate ions (0.027−0.243 M) were also present in the aqueous regions to more faithfully model a stream of uranyl-containing groundwater contacting a mineral system comprised of Na-smectite. No adsorption occurred near the pyrophyllite surface, and there was little difference in uranyl adsorption onto the beidellite and montmorillonite, despite the difference in location of clay layer charge between the two. At low uranyl concentration, the pentaaquouranyl complex dominates in solution and readily adsorbs to the clay basal plane. At higher uranyl (and carbonate) concentrations, the mono(carbonato) complex forms in solution, and uranyl adsorption decreases. Sodium adsorption onto beidellite occurred both as inner- and outer-sphere surface complexes, again with little effect on uranyl adsorption. Uranyl surface complexes consisted primarily of the pentaaquo cation (85%) and to a lesser extent the mono-(carbonato) species (15%). Speciation diagrams of the aqueous region indicate that the mono(carbonato)uranyl complex is abundant at high ionic strength. Oligomeric uranyl complexes are observed at high ionic strength, particularly near the pyrophyllite and montmorillonite surfaces. Atomic density profiles of water oxygen and hydrogen atoms are nearly identical near the beidellite and montmorillonite surfaces. Water structure therefore appears to be governed by the presence of adsorbed ions and not by the location of layer charge associated with the substrate. The water oxygen density near the pyrophyllite surface is similar to the other cases, but the hydrogen density profile indicates reduced hydrogen bonding between adsorbed water molecules and the surface.

* Corresponding author phone: 505 284 4895; fax: 505 744 7354; e-mail: jagreat@sandia.gov.

Introduction

The adsorption of dissolved species onto mineral surfaces is a critical process in the attenuation of chemical and radioactive contaminants in groundwater systems. The complex nature of soils, especially those involving clay minerals and other nanosized materials, makes it difficult to characterize and evaluate the extent to which contaminants are retarded. The evaluation of groundwater contamination by radionuclides requires accurate physical and chemical models of the partitioning of the radionuclide between groundwater and mineral. Uranium species derived from mining operations, mill tailings, nuclear tests, natural deposits, and potentially breached waste repositories are of particular importance. The uranyl ion (UO_2^{2+}) is the dominant uranium species found in contaminated groundwater systems and can occur at levels more than 100 ppb in the vicinity of uranium mill sites (*1*) (30 ppb is the U.S. Environmental Protection Agency maximum contaminant level for drinking water). Although field site analysis and laboratory experiments provide some measurement of the attenuation capacity of clay minerals for uranyl (*2*−*7*), there is still much to be learned about the specifics of adsorption and exchange mechanisms. Recent X-ray absorption fine structure (XAFS) studies of uranyl on mineral surfaces have helped in this effort by providing structural details of the surface complexes (*8*−*12*). However, there still exists a considerable gap of knowledge in our atomistic level understanding of uranyl adsorption onto mineral surfaces from aqueous solution.

Our goal is to provide an atomistic insight into the uranyl ion adsorption process in an effort to explain trends seen by experiment (*13*, *14*), namely that uranyl adsorption by smectite decreases with increasing pH. Metal ions associated with radioactive waste (Cs^+, Sr^{2+}, UO_2^{2+}) have received particular attention in the literature, but details obtained from their adsorption pathways should be applicable to other aqueous metals.

In a previous paper, we developed a methodology to perform large-scale simulations of uranyl ion adsorption onto an external montmorillonite surface (*15*). The aqueous regions contained uranyl ion and carbonate ion concentrations as low as 0.027 M in contact with an external montmorillonite surface. The constraint of charge neutrality required that uranyl ions be added to the aqueous region with anions. The carbonate ion was chosen because of its prevalence in natural groundwater (*16*) and because uranyl ion mobility is increased in the presence of aqueous carbonate (*17*). Percent ion adsorption was calculated from peaks in the atomic density profiles near the clay surface. We were then able to obtain standard-state Gibbs free energy and equilibrium constants for the ion adsorption process, including distribution coefficients (K_D). As $[UO_2^{2+}]$ and $[CO_3^{2-}]$ were increased from 0.027 to 0.162 M, calculated K_D values for uranyl adsorption decreased. Uranyl adsorption occurred in the presence of sodium ions, which were used to balance the negative layer charge of clay. Sodium K_D values were invariant with changes in $[UO_2^{2+}]$ and $[CO_3^{2-}]$. Increasing the solution ionic strength with additional sodium ions and carbonate ions resulted in further reduction of uranyl K_D and no change in sodium K_D. The trend in adsorption coincided with the tendency of uranyl ions to form aqueous carbonato complexes, which were less likely to interact with a negatively charged clay mineral. At such high uranyl and carbonate concentrations, uranyl precipitates are expected to appear (*18*). The small number of aqueous ions in our simulation systems prevented the formation of such distinct

10.1021/es052522q CCC: $33.50 © 2006 American Chemical Society
Published on Web 05/12/2006

phases, but uranyl oligomers formed that are precursors to solid phases (*15*).

This work continues the methodology discussed above, paying attention to the role of the clay mineral in the uranyl adsorption process. Specifically, the effect of layer charge was determined by including an uncharged clay (pyrophyllite), which allows the role played by the silicate surface in uranyl adsorption to be deduced. The effect of location of negative charge was considered by including uranyl adsorption onto beidellite, in which the negative charge resides much closer to the clay surface in the tetrahedral layer. An added benefit of this study allows the structure of water near charged and neutral clay surfaces to be compared. The presence of adsorbed ions and their solvation shells is also expected to alter the structure of interfacial water. Although the model system represents an idealized clay surface, insights into interfacial structure and ion adsorption equilibria should help in understanding these processes in heterogeneous media.

Methods

Our simulation methodology has been used previously (*15*) and will be briefly reviewed here. We employed the CLAYFF parameter set (*19*) that allows for full flexibility of tetrahedral and octahedral units in clay structures without the constraints of bond stretch and angle bending terms. This model addresses two critical issues in molecular models of beidellite, in which the negative charge resides primarily in the tetrahedral layer. The molecular flexibility of CLAYFF allows for distortion of AlO_4 units, and the −1 e charge at a tetrahedral or octahedral substitution site is almost completely delocalized among neighboring oxygen atoms (*19*). Polyatomic species in the aqueous regions are also fully flexible, because the model includes intramolecular force field parameters (angle bend, bond stretch). We incorporated the flexible SPC water model (*20*), upon which CLAYFF is based (*19*). Parameters for the flexible uranyl (*21*) and carbonate (*22*) ions were discussed previously (*15*).

The generic unit cell formula for the clay models in our simulations is $[Si_8](Al_4)O_{20}(OH)_4$, with Si and Al in tetrahedral and octahedral coordination, respectively. The model system was expanded into an orthorhombic clay lattice consisting of 8 × 4 repeats of the unit cell, with the formula $[Si_{256}](Al_{128})O_{640}(OH)_{128}$. A single clay layer is approximately 42 Å × 36 Å in the *x* and *y* dimensions, respectively. Three variations of the clay were used. Pyrophyllite consists of the lattice discussed above and possesses no net charge. Beidellite and montmorillonite were assigned charges of −0.75 e/unit cell through isomorphic substitution. Beidellite contained charge sites in the tetrahedral layer, $[Si_{232}Al_{24}](Al_{128})O_{640}(OH)_{128}$, and montmorillonite contained charge sites in the octahedral layer, $[Si_{256}](Al_{104}Mg_{24})O_{640}(OH)_{128}$. Charge sites were distributed randomly within the assigned sheet following the constraint of nearest-neighbor arrangements of Si−O−Al (tetrahedral) or Al−O−Mg (octahedral) linkages (*23*). The distribution of charge sites can be classified according to the number of nearest-neighbor metal ions surrounding each tetrahedral Si atom and the number of nearest neighbor metal ions surrounding each octahedral Al atom. The tetrahedral sheet of beidellite contained the ratio Al/Si = 1/9.7, having the charge sites distributed as follows: 30% of the Si atoms were surrounded by 2 Si atoms and 1 Al atom (2 Si + 1 Al), while 70% of the Si atoms were surrounded by 3 Si. Such a low portion of charge sites required every Al charge site to be surrounded by 3 nearest neighbor Si atoms (*23*). Each octahedral sheet in montmorillonite contained the ratio Al/Si = 1/4.3 with the following distribution about Al atoms: 10% (1 Al + 2 Mg); 50% (2 Al + 1 Mg); 40% (3 Al). There were no adjacent octahedral charge sites in the montmorillonite model.

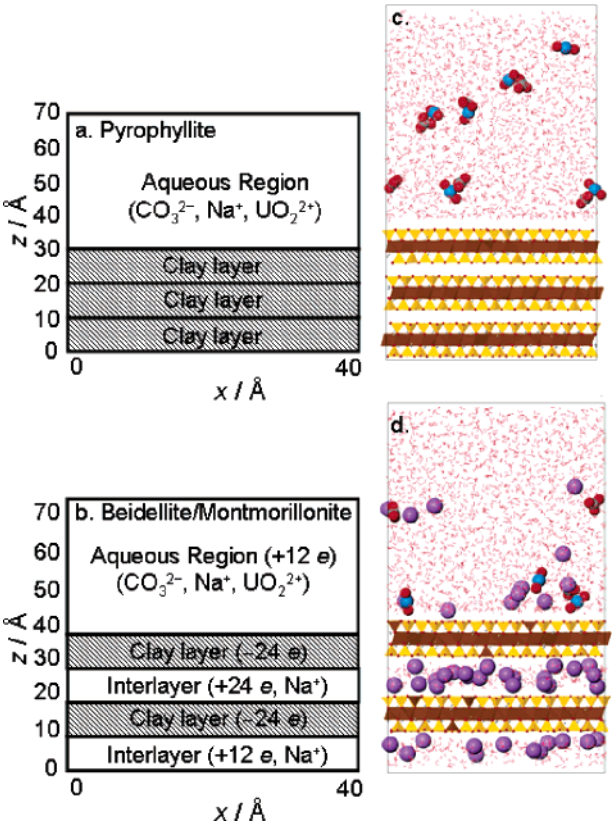

FIGURE 1. Schematic of the MD simulation cells containing (a) uncharged clay and (b) charged clay. The net atomic charge and location of aqueous ions in each region are shown in parentheses. The *y* dimension of the cell (not shown) is approximately 36 Å in length. Each region in the pyrophyllite system (a) is charge neutral. The aqueous regions could be further divided into adsorbed and diffuse layers. Molecular models are shown for (c) uncharged clay and (d) charged clay systems. Silica tetrahedra are colored gold, and alumina polyhedra are colored brown. Aqueous species are colored as follows: O (red); Na (purple); H (white); U (blue); C (gray).

The charged clays were balanced by interlayer regions consisting of aqueous sodium ions in a two-layer hydrate. An aqueous region approximately 40 Å thick was placed next to one clay layer. This 2000-particle region consisted of water molecules and ions (carbonate, sodium, and uranyl). Schematics of the model systems are shown in Figure 1. Two clay layers and two interlayers (8 × 4 × 2 unit cells) were used for the charged clays. For pyrophyllite, which has no layer charge and no interlayer water (*24*), three clay layers were used to approximate the same substrate thickness (8 × 4 × 3 unit cells). Sodium ions were added to the diffuse aqueous region to charge balance the clay layers, and one, three, and six pairs of uranyl and carbonate ions were added. From previous *NPT* (number density, pressure, temperature) MD simulations of these isolated aqueous regions, the approximate molar concentrations of $[UO_2CO_3]$ were found to be 0.027, 0.081, and 0.162 M (*15*). To examine the effect of increased ionic strength without changing $[UO_2^{2+}]$, a fourth set of simulations was conducted in which three carbonate ions and six sodium ions were added to the diffuse aqueous region. The carbonate ion concentration for this system was 0.243 M, while the uranyl ion concentration remained 0.162 M. While changes in $[CO_3^{2-}]$ are typically associated with changes in solution pH, our model ignores other pH-dependent effects such as water dissociation and protonation/deprotonation of clay surface sites. The presence of hydroxide ions would certainly result in new uranyl aqueous

complexes (*14*), but their effect on uranyl adsorption trends is uncertain. Also, this study is concerned with the basal siloxane surface of smectite clays, whose surface speciation is generally invariant to pH.

MD simulations were performed in the constant *NVT* (number of particles, volume, temperature) ensemble at 300 K using the LAMMPS software package (*25*). The thermostat relaxation time was 100 fs. Equilibration simulations were 0.1 ns in length, followed by production simulations of 1.0 ns. A two-level reversible reference system propagator algorithm (rRESPA) (*26*) was used. Long-range electrostatics were calculated every 2.0 fs using the particle−particle particle−mesh (PPPM) solver (*27*), while all other energy terms were calculated every 1.0 fs. A real-space cutoff of 10.0 Å was used for all short-range energy calculations. The model system was periodic in x and y, and slab periodic boundary conditions were used in the z direction, as discussed previously (*15*). Periodicity was included in the z direction, but a vacuum layer was inserted between repeats of the MD cell. The thickness of the vacuum layer was equal to three times the height of the MD cell, or approximately 210 Å. Additionally, Lennard-Jones (LJ) 9−3 walls located at $z = 0$ and at the upper end of the simulation cell (69.5 Å $\langle z \rangle$ 71.5 Å) prevented atoms from entering the vacuum region, and dipole interactions between adjacent MD cells were omitted (*25*). The simulated system was thus effectively two-dimensional while taking advantage of the efficient three-dimensional PPPM solver for long-range electrostatics.

One-dimensional atomic density profiles were collected during the 1.0-ns production simulations. The profiles from 10 such simulations (differing only in the initial configuration) were averaged to reflect 10 ns worth of data for each clay−solution combination. A total of 120 ns of production simulations were used in the analysis.

Results

Atomic density profiles are shown in Figures 2 and 3. Ion adsorption information was obtained from C, Na, and U profiles (Figure 2). Additionally, water density profiles (Figure 3) provide a unique insight into the effect of surface charge on interfacial water structure. The compactness of the clay layers is evident from the clay oxygen peaks in Figure 2; atomic density profiles for aluminum and silicon are not shown. Prominent ion peaks are seen for interlayer sodium ions as well as adsorbed sodium and uranyl ions. The uranium peaks near beidellite and montmorillonite basal surfaces (Figure 2b,c) are similar, indicating an identical adsorption pathway. Specifically, the O−U−O axis is tilted with respect to the surface normal, and the equatorial shell contains no surface O atoms (cf. Figure 1d and ref *15*). Atomic densities approach zero at $z = 0$ and $z = 70$ Å as a result of the LJ terminations. The termination at $z = 0$ had very little effect on the pyrophyllite structure (Figure 2a), but the effect is more pronounced for interlayer sodium ions (Figure 2b,c). Ions adsorbed onto pyrophyllite and montmorillonite formed single peaks approximately 4 Å from surface oxygen atoms, indicating outer-sphere complexation. The pentaaquouranyl complex is tilted with respect to the surface to promote hydrogen bonding between ligand water molecules and surface oxygen atoms. There are, however, no water molecules between uranyl O atoms and the surface. Atomic density profiles in the diffuse region (z > 40 Å) should be featureless with no peaks. However, at higher ionic concentrations broad peaks are observed, particularly for sodium and carbonate ions (Figure 2). This structure is partly due to the artificial solution−wall interface (z = 70 Å). At higher concentrations most cations formed complexes with carbonate ions, and these charged species tend to be repelled from the negative clay surfaces. The finite simulation times and small sample set (10 runs/concentration) could also

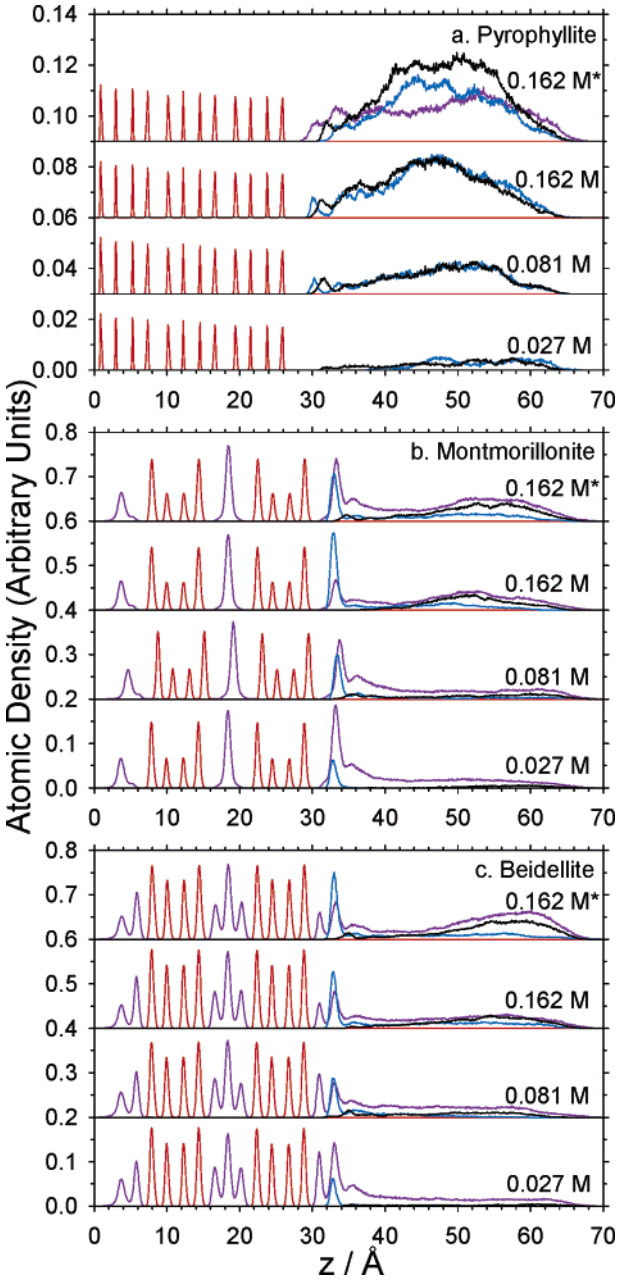

FIGURE 2. Atomic density profiles for aqueous ions and clay oxygen atoms. The color scheme is clay O (red), Na (purple), U (blue), and C (black). For each clay system, profiles are arranged in increasing [UO_2^{2+}]: 0.027 M (bottom), 0.081 M, and 0.162 M. In the top data set, denoted by an asterisk, additional sodium and carbonate ions were added to the aqueous region so that [Na^+] = 0.324 M and [CO_3^{2-}] = 0.243 M.

cause the irregular atomic density profiles. More simulations over longer times and with a significantly larger diffuse region would no doubt smooth the diffuse density profiles, but we would expect little change in the adsorbed ion density profiles.

Pyrophyllite. Uranyl adsorption peaks are present at intermediate uranyl concentrations only. Accompanying carbon peaks indicate the presence of UO_2CO_3 surface complexes (Figure 2a). When sodium ions were added to the aqueous region (top graph of Figure 2a), the sodium ions preferentially adsorbed while uranyl carbonato complexes remained in the diffuse region. The water oxygen densities near pyrophyllite (Figure 3) are similar to those near the charged clay surfaces. The hydrogen peak nearest the surface is reduced, indicating much less hydrogen bonding to the

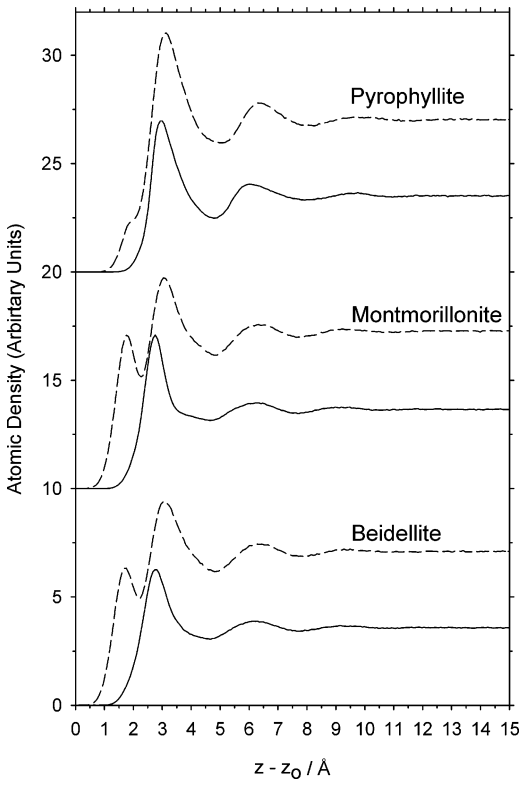

FIGURE 3. Atomic density profiles for water near each surface, where z_0 refers to the z coordinate of the nearest surface oxygen peak. Results are presented for 0.081 M UO_2CO_3, with water oxygen and hydrogen atoms shown as solid and dashed lines, respectively.

surface and increased hydrogen bonding among water molecules. The limited hydrogen bonding between water molecules and the pyrophyllite surface is a likely explanation for the difference in swelling behavior between pyrophyllite and charged clays.

Montmorillonite and Beidellite. The beidellite−solution interface is characterized by an additional sodium ion peak at approximately $z = 31$ Å (Figure 2c). Sodium ions formed both inner-sphere and outer-sphere surface complexes at the external surface as well as in the interlayer. Despite the difference in sodium ion adsorption, the structure of water near external surfaces of beidellite and montmorillonite is nearly identical (Figure 3). In both cases, the prominent water hydrogen peak at 1.7−1.8 Å indicates strong hydrogen bonding with surface oxygen atoms. Apparently, water structure is governed more by the presence of adsorbed ions and their hydration spheres than the location of negative charge sites. Unfortunately a "control simulation" consisting of pure water near these charged siloxane surfaces is not possible due to electroneutrality constraints of the simulation methods. Aqueous cations are always needed to balance the negative layer charge of the clay. A simplified model system consisting of a single clay charge site—and therefore only one aqueous cation—could help to highlight the effect of clay layer charge on interfacial water structure. However such an extension is beyond the scope of this work. The pyrophyllite−water interface is also a useful comparison, and Figure 3 shows little difference in the water oxygen density profiles between the uncharged (pyrophyllite) and charged clay interfaces.

Atomic density peaks were integrated to yield percent ion adsorption, as shown in Table 1. Integration boundaries were determined by the z coordinate at which the atomic density reached a minimum value. For ions adsorbing via outer-sphere surface complexation, the integration range was approximately 3.0 Å (Figure 2). For sodium ions adsorbing

TABLE 1. Percent Ion Adsorption at the External Clay Surface

		pyrophyllite		montmorillonite		beidellite	
[UO_2^{2+}]	[CO_3^{2-}]	% UO_2^{2+}	% Na^+	% UO_2^{2+}	% Na^+	% UO_2^{2+}	% Na^+
0.027	0.027	0		99	33	85	35
0.081	0.081	3		56	22	46	25
0.162	0.162	2		29	16	31	20
0.162	0.243	0	4	48	12	38	14

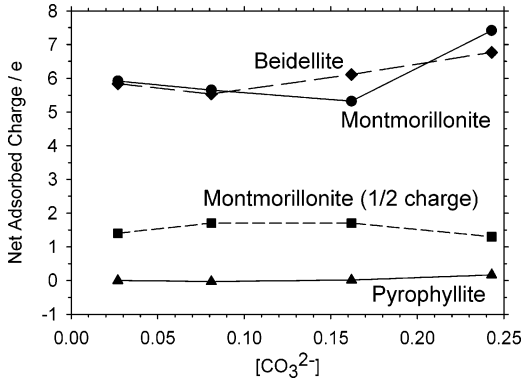

FIGURE 4. Net adsorbed charge due to carbonate, sodium, and uranyl ions for each of the three main clay systems. Results are also presented for a montmorillonite system in which the clay layer charge was reduced by half (*15*).

onto the beidellite surface, both inner- and outer-sphere peaks were included in the integrations. With no negative surface charge, ion adsorption onto pyrophyllite was almost nonexistent. A general pattern emerged for uranyl adsorption onto the charged clay surfaces: as uranyl concentration was increased, the percent adsorption decreased. If we keep in mind that carbonate ions accompanied uranyl ions in the aqueous region, the effect of uranyl carbonato complexes must be considered. Uranyl carbonato surface complexes accounted for approximately 15% of adsorbed uranyl (higher ionic strength), but they always coadsorbed with one or two sodium ions. When the solution ionic strength was increased with additional sodium and carbonate ions, uranyl adsorption then increased. The opposite trend was seen in our previous study of a reduced-charge montmorillonite, when uranyl adsorption continued to decrease even at this higher ionic strength (*15*). The magnitude of permanent clay charge does indeed affect uranyl adsorption, both in the relative amount of uranyl adsorbed and in the adsorption behavior at higher ionic strength. Sodium adsorption onto beidellite and montmorillonite remained relatively consistent despite changes in ionic strength. The presence of inner-sphere surface complexes near the beidellite surface resulted in a slightly higher sodium adsorption compared to montmorillonite and a significantly lower uranyl adsorption (10%) compared to montmorillonite ([CO_3^{2-}] = 0.027, 0.081, 0.243 M).

The results from Table 1 were used to calculate the net adsorbed charge near each external clay surface. As Figure 4 shows, montmorillonite and beidellite surfaces were effectively neutralized by +6 e in adsorbed ions. In the model systems, the beidellite and montmorillonite clay layers each bore a charge of −24 e, so the aqueous layer at each surface contained a total charge of +12 e (cf. Figure 1). The adsorbed layer therefore contained approximately 50% of the neutralizing charge. Our choice of units for surface and aqueous layer charge may be misleading, since the model system contained clay surfaces of infinite extent (periodic boundary conditions). The clay surface area was approximately 1490 Å^2, so the clay (+24 e) and adsorbed (+6 e) surface charges

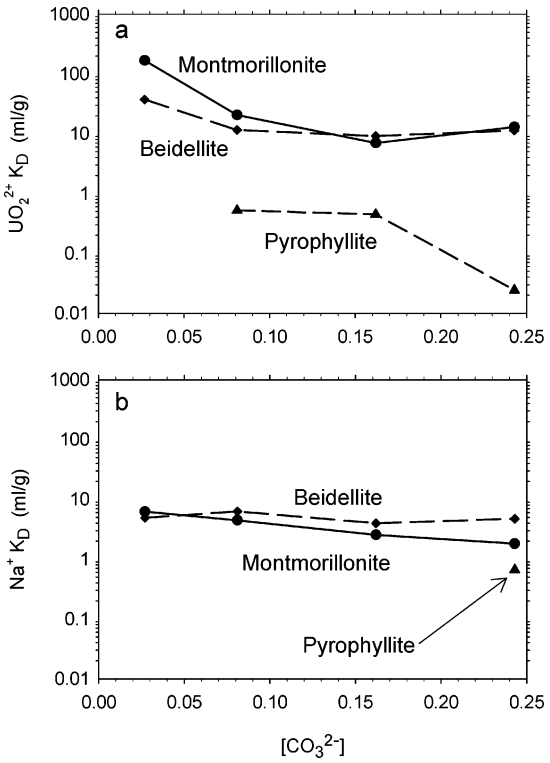

FIGURE 5. Cation adsorption tendencies expressed as equilibrium distribution coefficients (K_D). Results are presented for (a) uranyl and (b) sodium. The clay systems are denoted. No uranyl adsorption was seen near the pyrophyllite surface at $[CO_3^{2-}] = 0.027$ M. No data are shown for sodium adsorption onto pyrophyllite in the first three systems because no sodium ions were present.

were 0.016 e/Å^2 and 0.004 e/Å^2, respectively. The presence of adsorbed carbonate ions near the pyrophyllite surface resulted in slightly negative adsorbed layer charges. There was a slight increase in pyrophyllite adsorbed charge at higher ionic strength due to the presence of adsorbed sodium ions. The crossing of montmorillonite and beidellite adsorbed charges is due to changes in uranyl carbonato complexation, which is discussed below. Figure 4 also contains results from a reduced charge montmorillonite (−0.375 e/unit cell, ref *15*). The adsorbed layer charge never surpassed +2 e, even though +6 e would be needed to neutralize the clay charge. Fewer sodium ions were present in the aqueous region, so uranyl ions were more likely to form carbonato complexes. Such complexes have a nonpositive charge and were repelled by the negative clay surface (*15*).

Another use of Table 1 is the calculation of equilibrium distribution coefficients according to (*15*, *28*)

$$K_D = \frac{(\%\ M_{adsorbed})(z_{diffuse\ layer})}{(\%\ M_{diffuse})(z_{adsorbed\ layer})}\left(\frac{V_l}{m_s}\right) \quad (1)$$

where M refers to Na^+ or UO_2^{2+}, z refers to the z-dimension of each layer (cf. Figure 1), V_l is the volume of the aqueous layer, and m_s is the mass of clay substrate. Our method of determining these values has been discussed previously (*15*). Figure 5 shows the uranyl and sodium adsorption equilibria as a function of aqueous solution composition. Because two cations were present in the aqueous region, competitive adsorption effects can be observed. Effects of solution concentrations were more pronounced for uranyl than for sodium. Uranyl ions tended to form carbonato complexes at higher ionic strength (see below), which resulted in reduced adsorption. It is also interesting to note that the presence of inner-sphere sodium surface complexes near the beidellite

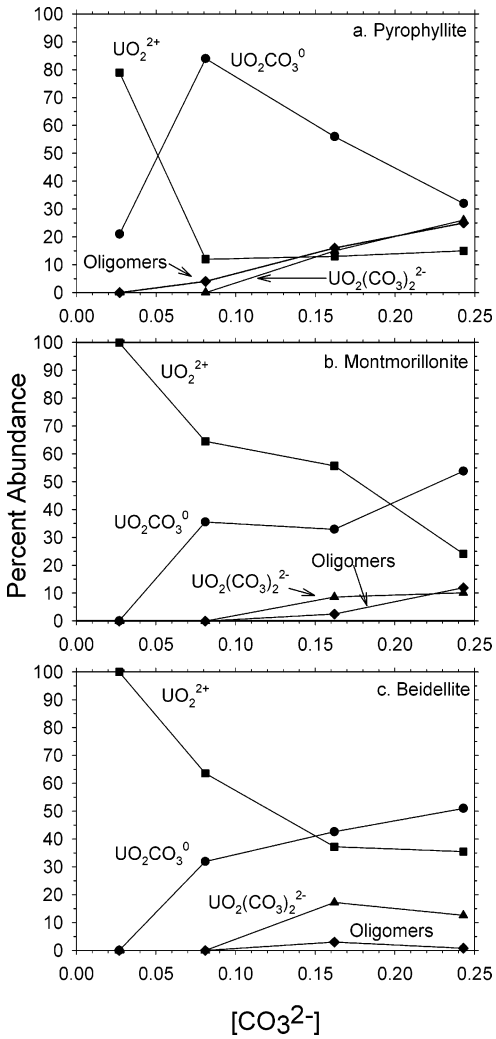

FIGURE 6. Uranyl speciation (first coordination shell) in the diffuse aqueous regions of (a) pyrophyllite, (b) montmorillonite, and (c) beidellite. The labeling scheme is $[UO_2(H_2O)_5]^{2+}$ (squares) denoted by UO_2^{2+}, $[UO_2(H_2O)_3(CO_3)]^0$ (circles) denoted by $UO_2CO_3^0$, $[UO_2(H_2O)(CO_3)_2]^{2-}$ (triangles) denoted by $UO_2(CO_3)_2^{2-}$, and oligomeric species (diamonds).

surface resulted in increased sodium adsorption compared to montmorillonite (Figure 5b). Although the uranyl concentrations in this study are orders of magnitude higher than those in batch adsorption experiments (*13*, *18*), the trends in uranyl K_D values are in agreement. Experimentally, uranyl adsorption onto montmorillonite increases as pH increases when $NaHCO_3$(aq) is used to buffer solution pH (*13*, *18*). In a carbonate-free system, the pH-dependence of uranyl adsorption depends on ionic strength (*29*). The effect of clay layer charge on uranyl adsorption is clearly seen in Figure 5a by comparing the pyrophyllite results with the other two. It should be noted that our simplified model only includes adsorption onto the external basal surfaces of clays. Ions can also adsorb onto the basal surfaces of the interlayer region as well as onto edge sites. Uranyl adsorption can be expected to occur at the edge sites of all clay minerals considered here because the protonation state of edge hydroxyl groups is pH dependent.

Speciation diagrams for diffuse uranyl ions (Figure 6) were prepared by examining 25 snapshots during each 1.0-ns simulation. The results in Figure 6 do not include adsorbed uranyl ions, which were mostly the pentaaquo species. At the lowest carbonate concentration (0.027 M), the pentaaquo uranyl complex was the dominant species. As $[UO_2CO_3]$ was

TABLE 2. Average Oxygen Coordination Numbers about U Atoms, Obtained by Integrating the First Peak in the Corresponding Radial Distribution Functions (*15*)

clay	$[CO_3^{2-}]$	U−O_w[a]	U−O_c[b]	tot. U−O
pyrophyllite	0.027	4.56	0.45	5.01
	0.081	3.23	1.78	5.01
	0.162	2.92	2.17	5.09
	0.243	2.58	2.74	5.32
montmorillonite	0.027	5.00	0.04	5.04
(1/2 charge)[c]	0.081	4.20	0.85	5.05
	0.162	3.30	2.00	5.30
	0.243	2.80	2.40	5.20
montmorillonite	0.027	5.00	0.00	5.00
	0.081	4.50	0.51	5.01
	0.162	4.42	0.63	5.05
	0.243	3.61	1.50	5.11
beidellite	0.027	5.00	0.00	5.00
	0.081	4.41	0.62	5.03
	0.162	3.87	1.21	5.08
	0.243	4.00	1.08	5.08

[a] Water oxygen. [b] Carbonate oxygen. [c] Reference 15.

increased, the mono(carbonato) complex appeared along with smaller amounts of the bis(carbonato) complex and oligomeric species. Examples of uranyl oligomers include $[(UO_2)_2(H_2O)_3(CO_3)_3]^{2-}$(aq) and $[(UO_2)_3(H_2O)_6(CO_3)_3]^0$(aq) (*15*). The tris(carbonato) complex accounted for less than 1% of the diffuse uranyl speciation and was not included in Figure 6. The high sodium content necessary for charge neutrality favored reduced formation of uranyl carbonato complexes compared to our previous study (*15*). As expected, carbonato complexes were more prevalent near the pyrophyllite surface, accounting for at least 85% of aqueous uranyl ions at all but the lowest concentration (Figure 6a). For the charged clays, reduced uranyl adsorption coincided with the emergence of carbonato complexes (Figure 6b,c). Additionally, the crossover in uranyl adsorption onto montmorillonite and beidellite between 0.162 and 0.243 M (Figures 4 and 5) can only be explained by considering uranyl speciation in the diffuse layer or the presence of inner-sphere sodium surface complexes near beidellite. For beidellite and montmorillonite, the percent abundance of carbonato complexes is quite similar. The difference in pentaaquo abundance correlates with the amount of uranyl adsorbed onto each surface (Table 2). At $[CO_3^{2-}] = 0.162$ M, more uranyl is adsorbed onto beidellite than montmorillonite (31% vs 29%), while the pentaaquo uranyl complex is less abundant in the diffuse region near beidellite than montmorillonite (37% vs 56%). At $[CO_3^{2-}] = 0.243$ M, more uranyl is adsorbed onto montmorillonite than beidellite (48% vs 38%), while the pentaaquo uranyl complex is less abundant in the diffuse region near montmorillonite than beidellite (24% vs 36%). The general result is that the amount of adsorbed uranyl is inversely proportional to the abundance of pentaaquo uranyl complex in the diffuse layer. Although uranyl speciation in the beidellite system appears to reach a steady-state at higher concentrations, uranyl and sodium carbonate solid phases would most likely form at higher carbonate ion concentrations (*16*).

The absence of the tris(carbonato) complex seems to disagree with experimental speciation diagrams (*18*), which assume a constant uranyl concentration (usually at micromolar concentrations) while the pH or carbonate ion concentration is varied. Due to the constraint of charge neutrality in our simulations, an increase in uranyl ion concentration was always accompanied by an equivalent increase in carbonate ion concentration. A local aqueous environment consisting of a single uranyl ion and multiple carbonate ions would likely result in increased abundance of the tris(carbonato)uranyl complex.

Trends in uranyl speciation were verified using radial distribution functions, which tabulate the local atomic density about different atom types (*30*). Radial distribution functions of U−O pairs were used to quantify the presence of carbonato ligands within the equatorial shell about uranyl ions. The interatomic distance at a peak height represents the mean distance between a shell of atoms and the central atom. For U−water O and U−carbonate O distributions, the average distances were 2.5 and 2.4 Å, respectively. The first peak in the U−O distributions were integrated to yield U−O coordination numbers, as shown in Table 2. The pentaaquo and mono(carbonato) complexes both result in U−O coordination numbers of 5. This value can increase upon formation of tris(carbonato) or oligomeric complexes. In general, carbonato ligands gradually replaced aquo ligands as the ionic strength increased. The degree of carbonato complexation was substantially greater in the pyrophyllite system. Results are also presented from the reduced-charge montmorillonite considered previously (*15*), which shows U−O coordination that is intermediate between the uncharged clay (pyrophyllite) and fully charged montmorillonite systems. Radial distribution functions of Na−O pairs confirm that inner-sphere sodium surface complexes are located near aluminum substitution sites. Inner-sphere sodium ions occupy sites near the three siloxane oxygen atoms near the aluminum site. The Na−O distance is approximately 2.3 Å, compared to an average distance of 3.8 Å between inner-sphere sodium and other siloxane oxygen sites. These results are in agreement with interlayer sodium ion adsorption near tetrahedral substitution sites (*31*). Uranyl ions, which only adsorbed onto beidellite as outer-sphere complexes, showed no preference for tetrahedral silicon or aluminum sites. The presence of tetrahedral charge sites in beidellite indirectly causes reduced uranyl adsorption because additional sodium ions are adsorbed to the surface through an inner-sphere mechanism.

The simulation methodology used in this study allowed for a comparison of water structure near the siloxane surfaces of clays as well as competitive adsorption between sodium ion and uranyl ions. The structure of water and ions near external clay surfaces leads to the general conclusion that the location of negative charge sites within clay layers has no significant effect on water structure but an indirect effect on ion adsorption. However, the presence of surface charge, compared with a neutral surface, results in considerable differences in interfacial structure. The pyrophyllite−water interface is unique in two ways: there is reduced hydrogen bonding between adsorbed water molecules and the surface (Figure 2), and there is reduced uranyl adsorption (Figure 5).

The interaction of aqueous uranyl carbonate solutions with external surfaces of beidellite and montmorillonite can be summarized as follows:

Low $[UO_2]$. At very low concentrations (essentially infinite dilution), the pentaaquo species dominates. Because $[UO_2(H_2O)_5]^{2+}$(aq) is the primary vehicle for uranyl adsorption, K_D values for charged clays are at their maximum values at low uranyl concentration. Near the pyrophyllite surface, some carbonato complexation occurs but no uranyl adsorption occurs.

Intermediate $[UO_2CO_3]$. The aqueous mono(carbonato) complex readily forms, resulting in a dramatic decrease in uranyl adsorption to 50% or less. The aqueous environment near the clay surface appears to be the main controlling factor in uranyl adsorption.

High Ionic Strength, or $[CO_3^{2-}] > [UO_2^{2+}]$. As the aqueous region is inundated with sodium and carbonate ions, the abundance of uranyl mono(carbonato) complexes increases, and in general uranyl adsorption decreases. The exception

is the beidellite system, in which both pentaaquo abundance and uranyl adsorption had already reached plateau values. These results confirm the hypothesis that uranyl adsorption onto the siloxane surface of clay minerals is electrostatic in nature. Adsorbed uranyl ions maintain their 5-fold oxygen coordination shells, consisting of mainly water but with small occurrence of carbonato ligands. The montmorillonite surface has a slightly higher affinity for aqueous uranyl adsorption in the presence of aqueous sodium ions. Sodium and other competing ions that can form inner-sphere surface complexes at tetrahedral charge sites will result in reduced uranyl adsorption.

Acknowledgments

We thank R. T. Pabalan for a critical review of the manuscript draft. We acknowledge support from the U.S. Department of Energy, Office of Basic Energy Sciences, Geosciences Research. Sandia is a multiprogram laboratory operated by Sandia Corp., a Lockheed Martin company, for the U.S. Department of Energy under Contract DE-AC04-94AL85000.

Literature Cited

(1) Zielinski, R. A.; Chafin, D. T.; Banta, E. R.; Szabo, B. J. Use of 234U and 238U isotopes to evaluate contamination of near-surface groundwater with uranium-mill effluent: A case study in south-central Colorado, USA. *Environ. Geol.* **1997**, *32*, 124−136.

(2) Barnett, M. O.; Jardine, P. M.; Brooks, S. C.; Selim, H. M. Adsorption and transport of uranium(VI) in subsurface media. *Soil Sci. Soc. Am. J.* **2000**, *64*, 908−917.

(3) Curtis, G. P.; Fox, P.; Kohler, M.; Davis, J. A. Comparison of in situ uranium K_D values with a laboratory determined surface complexation model. *Appl. Geochem.* **2004**, *19*, 1643−1653.

(4) Hyun, S. P.; Cho, Y. H.; Hahn, P. S.; Kim, S. J. Sorption mechanism of U(VI) on a reference montmorillonite: binding to the internal and external surfaces. *J. Radioanal. Nucl. Chem.* **2001**, *250*, 55−62.

(5) Kohler, M.; Curtis, G. P.; D. E., M.; Davis, J. A. Methods for estimating adsorbed uranium(VI) and distribution coefficients of contaminated sediments. *Environ. Sci. Technol.* **2004**, *38*, 204−247.

(6) McAlister, J. J.; Cooney, G.; Higgins, M. J. Accumulation of uranium in granitic soils overlying the Mourne Mountains, County Down, Northern Ireland. *Microchem. J.* **1997**, *56*, 1997.

(7) Sylwester, E. R.; Hudson, E. A.; Allen, P. G. The Structure of uranium (VI) sorption complexes on silica, alumina, and montmorillonite. *Geochim. Cosmochim. Acta* **2000**, *64*, 2431−2438.

(8) Greathouse, J. A.; StellaLevinsohn, H. R.; Denecke, M. A.; Bauer, A.; Pabalan, R. T. Uranyl surface complexes in a mixed-charge montmorillonite: Monte Carlo computer simulation and polarized XAFS results. *Clays Clay Miner.* **2005**, *53*, 278−286.

(9) Giaquinta, D. M.; Soderholm, L.; Yuchs, S. E.; Wasserman, S. R. The speciation of uranium in a smectite clay: evidence for catalysed uranyl reduction. *Radiochim. Acta* **1997**, *76*, 113−121.

(10) Hudson, E. A.; Terminello, L. J.; Viani, B. E.; Denecke, M.; Reich, T.; Allen, P. G.; Bucher, J. J.; Shuh, D. K.; Edelstein, N. M. The structure of U^{6+} sorption complexes on vermiculite and hydrobiotite. *Clays Clay Miner.* **1999**, *47*, 439−457.

(11) Walter, M.; Arnold, T.; Reich, T.; Bernhard, G. Sorption of uranium(VI) onto ferric oxides in sulfate-rich acid waters. *Environ. Sci. Technol.* **2003**, *37*, 2898−2904.

(12) Denecke, M. A.; Dardenne, K.; Lindqvist-Reis, P.; Rothe, J. Grazing incidence XAFS investigations of Hf(IV) and U(VI) cations sorbed onto mineral surfaces. *Phys. Chem. Chem. Phys.* **2003**, *5*, 939−946.

(13) Ames, L. L.; McGarrah, J. E.; Walker, B. A. Sorption of trace constituents from aqueous solutions onto secondary minerals. I. Uranium. *Clays Clay Miner.* **1983**, *31*, 321−334.

(14) Pabalan, R. T.; Turner, D. R.; Bertetti, F. P.; Prikryl, J. D. Uranium(VI) sorption onto selected mineral surfaces. In *Adsorption of Metals by Geomedia*; Jenne, E., Ed.; Academic Press: New York, 1998; pp 99−130.

(15) Greathouse, J. A.; Cygan, R. T. Molecular dynamics simulation of uranyl(VI) sorption equilibria onto an external montmorillonite surface. *Phys. Chem. Chem. Phys.* **2005**, *7*, 3580−3586.

(16) Clark, D. L.; Hobart, D. E.; Neu, M. P. Actinide carbonate complexes and their importance in actinide environmental chemistry. *Chem. Rev.* **1995**, *95*, 25−48.

(17) Ragnarsdottir, K. V.; Charlet, L. In *Winter Meeting of the Mineralogical Society of Great Britain and Ireland*; CotterHowells, J. D. C., L. S., ValsamiJones, E., Batchelder, M., Eds.; Mineralogical Society Great Britain and Ireland: London, 1999; Vol. 9, pp 245−289.

(18) Pabalan, R. T.; Turner, D. R. Uranium (6+) sorption on montmorillonite: experimental and surface complexation modeling study. *Aquat. Geochem.* **1997**, *2*, 203−226.

(19) Cygan, R. T.; Liang, J.-J.; Kalinichev, A. G. Molecular models of hydroxide, oxyhydroxide, and clay phases and the development of a general force field. *J. Phys. Chem. B* **2004**, *108*, 1255−1266.

(20) Teleman, O.; Jonsson, B.; Engstrom, S. A molecular dynamics simulation of a water model with intramolecular degrees of freedom. *Mol. Phys.* **1987**, *60*, 193−203.

(21) Guilbaud, P.; Wipff, G. Force field representation of the UO_2^{2+} cation from free energy MD simulations in water. Tests on its 18-crown-6 and NO_3^- adducts, and on its calix[6]arene^{6-} and CMPO complexes. *J. Mol. Struct.* **1996**, *366*, 55−63.

(22) Greathouse, J. A.; O'Brien, R. J.; Bemis, G.; Pabalan, R. T. Molecular dynamics study of aqueous uranyl interactions with quartz (010). *J. Phys. Chem. B* **2002**, *106*, 1646−1655.

(23) Heinz, H.; Suter, U., W Surface structure of organoclays. *Angew. Chem., Int. Ed.* **2004**, *43*, 2239−2243.

(24) Newman, A. C. D.; Brown, G. The chemical constitution of clays. In *Chemistry of Clays and Clay Minerals*; Newman, A. C. D., Ed.; Longman Group, Ltd.: Harlow, U.K., 1987; Vol. 6, pp 1−128.

(25) Plimpton, S. J. Fast parallel algorithms for short-range molecular dynamics. *J. Comput. Phys.* **1995**, *117*, 1−19.

(26) Tuckerman, M. E.; Martyna, G. J.; Berne, B. J. Molecular dynamics algorithms for condensed systems with multiple time scales. *J. Chem. Phys.* **1990**, *93*, 1287−1291.

(27) Plimpton, S. J.; Pollock, R.; Stevens, M. In *Eighth SIAM Conference on Parallel Processing for Scientific Computing*; 1997.

(28) Zangi, R.; Engberts, J. B. F. N. Physisorption of hydroxide ions from aqueous solution to a hydrophobic surface. *J. Am. Chem. Soc.* **2005**, *127*, 2272−2276.

(29) McKinley, J. P.; Zachara, J. M.; Smith, S. C.; Turner, G. D. The influence of uranyl hydrolysis and multiple site-binding reactions on adsorption of U(VI) to montmorillonite. *Clays Clay Miner.* **1995**, *45*, 586−598.

(30) Allen, M. P.; Tildesley, D. J. *Computer Simulation of Liquids*; Clarendon Press: Oxford, U.K., 1987.

(31) Chang, F.-R. C.; Skipper, N. T.; Sposito, G. Computer simulation of interlayer molecular structure in sodium montmorillonite hydrates. *Langmuir* **1995**, *11*, 2734−2741.

Received for review December 16, 2005. Revised manuscript received April 11, 2006. Accepted April 12, 2006.

ES052522Q